This article has been accepted for publication in a future issue of this journal, but has not been fully edited. Content may change prior to final publication. Citation information: DOI 10.1109/JSEN.2018.2822290, IEEE Sensors Journal

# Periodic pulsed thermography for inner defects detection of lead-steel bonded structure

Xiaoxi Li[1], Bin Gao[1], Yuyu Zhu[1], Wai Lok Woo[2], Guiyun Tian[1,2], Guangping Tang[3], Jianwen Li[3], Chaoming Sun[3]

[1]*School of Automation Engineering, University of Electronic Science and Technology of China, Chengdu, China*

[2]*School of Electrical and Electronic Engineering, Newcastle University, England, United Kingdom*

[3]*China Academy of Engineering Physics, Mianyang, China*

*Corresponding author: bin_gao@uestc.edu.cn*

***Abstract*—Multilayer materials with metal-metal bonded structure have been widely applied in aviation, aerospace, and nuclear industry. Disbond is prone to exist in lead-steel bonded structure, which degrades the load capacity and mechanical behaviors. Thermography nondestructive testing is a potential candidate for sub-layer defect detection. However, lead-steel bonded structure is unbearable when undertaken with over-heating of instantaneous temperature, which will lead to subsequent damage or generation of more unpredictable disbond. In addition, detection sensitivity of the deeper defects requires to be enhanced. In this paper, the mathematical derivation and the implementation of the periodic pulsed thermography have been established for detecting inner defects of lead-steel structure. This has been especially conducted for detecting small and deep defects that require high energy to increase detectability. Validation of the proposed method has been undertaken on both inductive thermography and optical thermography. The obtained results have demonstrated that periodic pulsed thermography is highly efficient for deep inner defect inspection of metal-metal bonded structure.**

***Index Terms*—Periodic pulsed thermography, lead-steel bonded structure, disbond defect, NDT&E.**

## I. Introduction

LEAD-STEEL bonded structure has characteristics of anti-nuclear radiation, high strength and anti-fatigue, which has been widely applied in nuclear industrial fields. However the bonded structure is prone to exist poor bonding, voids, porosity, and disbond defect during the manufacturing process as well as in service stage. These defects damage the integrity of the bonding structure, which can lead to the degradation of the load capacity and mechanical behaviors, even to radiation leakage [1-3]. Therefore, it is essential to develop a reliable non-destructive test (NDT) method to assess the bonding quality and guarantee safety.

Detection for lead-steel bonded structure has two challenges: complex multi-layer structure and thickness. Extensive studies have been carried out to evaluate adhesive quality of the bonding structures [4-5]. The magnetic particle testing has limited penetration and will contaminate the specimen [6]. Ultrasonic testing (UT) based on the propagation of ultrasonic waves in the object has good detectability for inner defects. However, common UT method requires couplant while this is not allowed by the nuclear industry in detecting lead-steel sample [7-8]. Laser Ultrasonic NDT has a good detection resolution for inner defects. However, it requires an ideal operating environment to guarantee the inspection quality, which is limited for the on-line detection. X-ray CT has high detectability for inner defects and can be used to quantitatively measure the depth of the defect [9]. However, X-ray cannot be applied in detecting lead-steel structure due to its limited penetration on the lead layer. Eddy current test has high sensitivity to surface crack for conductive material inspection. However, it is difficult to access the inner defect because of the limitation of the penetration. Therefore, the Infrared (IR) thermography NDT is a potential candidate to inspect this kind of structures because of its ability of noncontact and fast as well as wide inspection [10-12]. The system of thermography NDT can realize portability and miniaturization, which is propitious to the on-line detection.

Active Infrared (IR) thermography can be divided into diverse modes depending on the extern stimulus such as pulsed thermography (PT), square pulsed thermography (SPT), step heating thermography (SHT), and lock-in thermography (LT) [13-17]. This can be summarized to two categories: transient mode and steady-state mode. Transient mode pays attention to transient changes in temperature, while the steady-state mode focuses on the steady-state changes in temperature. A strategy is built to combine the advantages of both modes in order to obtain more effective information to improve detection sensitivity. These include pulsed phase thermography (PPT), [18-19], frequency modulated thermal wave thermography [20], and code pulses thermography [21-22].

In this work, the task is to detect inner defects in the lead-steel structure. In transient mode, a long pulse is required to inspect the smaller or deeper defects due to physical property of the structures. However, the bonding layer and lead part of this structures is not allowed to withstand over-heating as instantaneous temperature rise. Therefore, a periodic pulsed thermography NDT as a combination of transient mode and steady-state mode is proposed.

This article has been accepted for publication in a future issue of this journal, but has not been fully edited. Content may change prior to final publication. Citation information: DOI 10.1109/JSEN.2018.2822290, IEEE Sensors Journal

Periodic pulsed thermography can detect smaller and deeper defects without damaging the adhesive. This is due to that it delivers adjustable energy to specimen while avoids instantaneous temperature rise. The theoretical derivation and verification have been conducted and a matched data processing method has been analyzed. Concurrently, the signal resolution has been improved due to the periodic attribute. According to the results of experiment, this method can detect least size of 4mm at depth of 1mm, and disbond defects at the second layer, whose depth is 5mm under the surface. In addition, one of the main strengths of the periodic pulsed thermography is that it is able to provide the setting of the minimum cycle, as the defects with different depth will influence different frequency response. Secondly, compared with the lock-in thermography system, periodic pulsed thermography system can be simply established by adjusting the pulsed thermography system.

The outline of the work is organized as follows: Section II describes the theory derivation of periodic pulsed thermography and introduces the data processing method. In addition, systems of both eddy current thermography (ECT) and optical thermography (OT) have been applied. Section III describes the simulation with COMSOL Multiphysics. Sections IV and V present the results of experimental work and detailed discussion as well as comparison. Finally, Section VI presents the conclusion and future work.

## II. THEORY AND METHODOLOGY

### A. Mathematical model of periodic pulsed thermography

Periodic pulsed thermography adopts periodic pulse to stimulate the specimen and consequently obtains a modulated temperature rise. The periodic pulse can be written in the following expression:

$$\begin{cases} q(t) = q(t + nT_0) \qquad n = 0,1,2,3\cdots \\ q(t) = \begin{cases} 0, 0 < t \le \dfrac{T_0}{2} \\ q_0, \dfrac{T_0}{2} < t \le T_0 \end{cases} \end{cases} \tag{1}$$

where $q(t)$ is the heat power, $q_0$ is the amplitude, $T_0$ is the period and $t$ is the heating time. This periodic function can be analyzed using the Fourier expansion:

$$q(t) = \frac{q_0}{2} + \frac{2q_0}{\pi}\sum_{k=1}^{+\infty}\frac{1}{2k-1}\sin((2k-1)\omega t) \tag{2}$$

$$\omega = \frac{2\pi}{T_0} \tag{3}$$

where $\omega$ is an angular frequency. When the specimen is heated, the heat flux can be considered as two parts depending on the linear superposition principle i.e., constant heat flux $\frac{q_0}{2}$ which produces the increase in temperature, and harmonic heat flux which produces harmonic thermal modulation.

According to the theory of thermal conduction [23], the steady state solution for single frequency harmonic heat flux in an isotropic and homogeneous material is represented in (4). This supposes infinite depth and the plane thermal wave propagating along with the depth direction.

$$\begin{aligned} T(z,t) &= A\exp(-z\sqrt{\frac{i\omega c\rho}{k}})e^{i\omega t} \\ &= A\exp(\frac{-z}{\Lambda})\exp(i(\omega t - \frac{z}{\Lambda})) \end{aligned} \tag{4}$$

$$\Lambda = \sqrt{\frac{2k}{\rho c\omega}} = \sqrt{\frac{2\alpha}{\omega}} \tag{5}$$

where $\alpha = k/(\rho c)$ is the thermal diffusion coefficient, $k$ is the heat conductivity, $\rho$ is the density, $c$ is the specific heat at constant pressure and $z$ is the depth. The quantity $\Lambda$ is the so-called thermal diffusion length. The amplitude factor $A$ can be obtained from amplitude of the surface power density $q_0$ by calculating the heat flux through the surface at the $z = 0$, namely

$$\begin{aligned} q_0 e^{(i\omega t + i\varphi)} &= -k\left.\frac{\partial T}{\partial z}\right|_{z=0} \\ &= A\sqrt{k\omega\rho c}\,e^{(i\omega t + i\varphi)} \end{aligned} \tag{6}$$

$$A = \frac{q_0}{\sqrt{k\omega\rho c}} \tag{7}$$

On the surface, the solution to single frequency harmonic heat flux at frequency $\omega$ is shown in (8):

$$T(0,t)_\omega = A\exp(i\omega t) \tag{8}$$

Similarly, the steady state solution for multi-frequency harmonic heat flux of $q(t)$ can represent as (9).

$$T(0,t)_S = \frac{2Aq_0}{\pi}\sum_{k=1}^{+\infty}\frac{1}{2k-1}\exp(i(2k-1)\omega t) \tag{9}$$

The transient state solution can be obtained by partial differential equations due to constant heat flux.

$$\rho c\frac{\partial T(z,t)_T}{\partial t} = \frac{p_0}{2} - \frac{T(z,t)_T - T_{am}}{R_{th}} \tag{10}$$

where $R_{th}$ is the thermal resistance of sample material. The transient solution of $q(t)$ is written as follows:

$$T(0,t)_T = T_{am} + \Delta T(1 - e^{-t/\tau}) \tag{11}$$

where $\tau = \rho c R_{th}$ denotes time constant, and $\Delta T = {}^{p_0}\!/_{2} \times R_{th}$

As discussed above, the solution of $T(0,t)$ is obtained by linear superposition principle:

$$T(0,t) = T(0,t)_T + T(0,t)_S \tag{12}$$

### B. Fourier analysis

Fourier Transform is applied to analyze the thermal image sequences of the periodic pulsed thermography.

$$F(f) = \Delta t\sum_{n=0}^{N-1}T[n\Delta t]e^{-i2\pi fn\Delta t} = R(f) + iI(f) \tag{13}$$

where $\Delta t$ is the sampling time step, $R(f)$ and $I(f)$ are the real and imaginary components of $F(f)$, respectively. The amplitude and phase spectrum were computed by using (14) and (15), respectively.

This article has been accepted for publication in a future issue of this journal, but has not been fully edited. Content may change prior to final publication. Citation information: DOI 10.1109/JSEN.2018.2822290, IEEE Sensors Journal

$$\varphi(f) = \tan^{-1}\left[\frac{I(f)}{R(f)}\right] \quad (14)$$

$$A(f) = \sqrt{R(f)^2 + I(f)^2} \quad (15)$$

### C. Exciting modes

In this paper, two types of stimulation source have been selected to heat the specimen: eddy current and optical. Eddy current stimulation drives an excitation coil with high frequency current above the conductive material. The current in the coil then induces an eddy current in conductive material. Due to the skin effect, the density of eddy current decreases sharply under the surface. The skin depth $\delta$ is defined as the depth when the eddy current density decreases to $1/e$ of the surface:

$$\delta = \frac{1}{\sqrt{\pi\mu\sigma f}} \quad (16)$$

where $\mu$ is magnetic permeability, $\sigma$ is the electrical conductivity, $f$ is the excitation frequency. Eddy current produce joule heat as an inner heat source. The heating depth $\delta th$ is defined as the depth when the heating power decreased to 1/e of the surface:

$$\delta th = \frac{1}{2\sqrt{\pi\mu\sigma f}} = \frac{1}{2}\delta \quad (17)$$

Three heating modes can be deduced depending on the $\delta th$, 1) surface or subsurface heating when $\delta th$ far less than the thickness of specimen, 2) local volume heating when $\delta th$ is unable to ignore but less than thickness of specimen, and 3) volume heating when $\delta th$ exceed the thickness of specimen.

Optical stimulation utilizes Halogen lamp to heat the specimen on the surface. The whole process consists only of heat conduction which satisfies the thermal wave conduction theory.

## III. Simulation Studies

In order to verify the detection feasibility of the periodic pulsed thermography for lead steel bonded structure, the numerical studies were conducted using multiphysics finite element modeling (FEM) software COMSOL Multiphysics 5.0.

### A. Simulation model and result in ECT

Three Dimensional (3D) numerical modeling of induction heating of bonding structures was performed in Fig.1. The size of structure is constant as $120mm \times 70mm$. The thickness of the first lead layer L1 and the second lead layer L2 is 1mm. The thickness of the first steel layer S1 and the second steel layer S2 is 4mm. They are bonded by adhesive layers E1, E2, and E3, respectively, which is set as 0.2mm. The excitation copper tube coil was modelled by outer diameter of 7mm and internal diameter of 5mm. Defects were modelled by the air gap. The lift-off distance between the coil and the surface of structure is 0.5mm. The entire domain was enclosed in the truncated air boundary with a constant surrounding temperature of 293K.

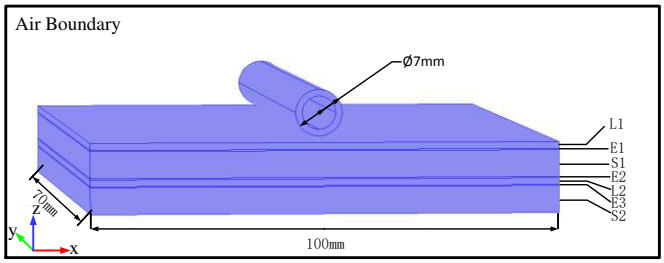


Fig.1 3D geometry of the lead-steal bonding structure

Table I illustrates the material parameters in simulation. The inner disbond defect is simulated by using a circular block with thickness of 0.2mm and diameter of 5mm, located in the center of the bonded layer.

TABLE I
MATERIAL PARAMETERS

| Parameters | Steel | lead | Epoxy |
|---|---|---|---|
| Relative permeability | 200 | 1 | 1 |
| Relative permittivity | 1 | 1 | 1 |
| Conductivity[$S/m$] | 5.5e6 | 4.84e6 | 10 |
| Heat capacity[$J/[kg*K]$] | 475 | 127 | 1255 |
| Density [$kg/m^3$] | 7850 | 11340 | 1260 |
| Thermal conductivity[$W/[m*K]$] | 51.9 | 35.3 | 0.2 |
| Thermal diffusivity[$m^2/s$] | 1.39e-5 | 2.45e-5 | 0.00138 |

The free tetrahedral has been selected to mesh the model as shown in the Fig.2. An external current of 380A at a frequency with 251 kHz was selected. The generated eddy current in the specimen were evaluated by using Maxwell's equation and the heat diffusion can be defined by using general heat transfer equation. Heating and cooling analysis for duration of T/2 were alternately used to the model as a pulse. T is the cycle. The selection of integration method and convergence analysis were finished automatically by the COMSOL.

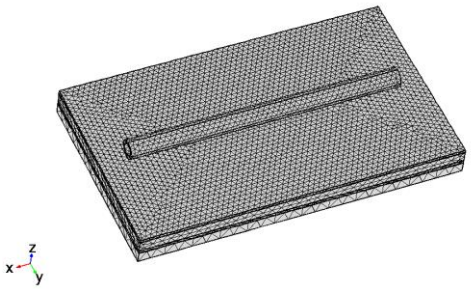


Fig.2 The meshing result

In simulation, single pulse with cycle of 6s, two pulses with cycle of 3s and three pulses with cycle of 2s were chosen as the same energy is applied. The sampling frequency is 50 Hz. According to lead property, the skin depth and the heating depth of lead is 0.457mm and 0.228mm, respectively. It is less than the thickness of the specimen but unable to ignore, belonging to local volume heating. The depth of defect is located at 1mm under the surface. Thus, the density of eddy current at depth of 1mm is too small. An internal heat source cross-section under the excitation coil through the specimen is shown in Fig.3(a).

This article has been accepted for publication in a future issue of this journal, but has not been fully edited. Content may change prior to final publication. Citation information: DOI 10.1109/JSEN.2018.2822290, IEEE Sensors Journal

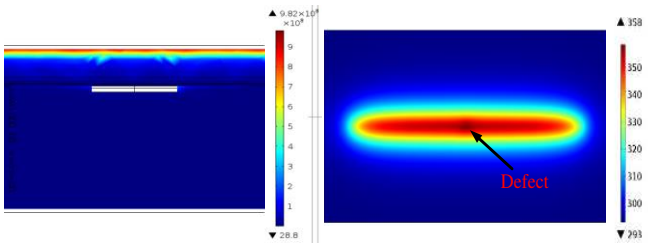


(a) (b)

Fig.3 (a) Internal heat source cross-section of ECT; (b) Thermal image in ECT

In Fig.3 (a), the red marked region represents the internal heat source. The white marked region represents the defect area. It represents that the area of eddy current heating appeared on the near surface due to the eddy current penetration depth. As penetration depth is significant small, the disturbance of the defect to the eddy current is negligible. The eddy current plays the role of internal heat source and the heat conduction dominates in detection of lead steel bonded structure. The thermal image is shown in Fig.3 (b). The defect area has a higher temperature. The transient temperature response at a pixel allocated in the defective area has been analyzed, which is shown in Fig.4.

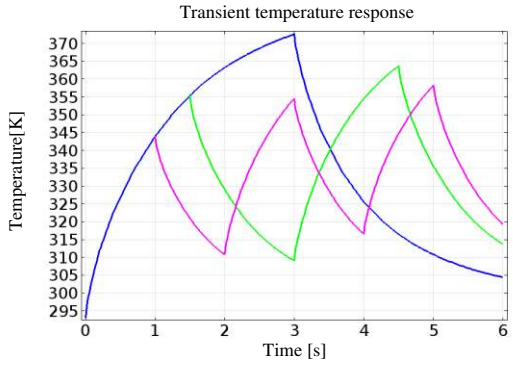


Fig.4 Transient temperature response in ECT

In Fig.4, the blue line describes the transient temperature response of one pulse, the green and pink lines illustrate the transient temperature response of two pulses and three pulses, respectively. The maximum temperature rise of two pulses decreases by 11% compared to one pulse, and by 17% in the case of three pulses.

### *B. Simulation model and result in OT*

In OT, the 3D geometry of the lead-steal bonding structure is the same. However, the coil is replaced by the inward heat flux, which is injected onto the surface to simulate optical heating. In thermal image, the defect area is shown as a hot zone as shown in Fig.5.

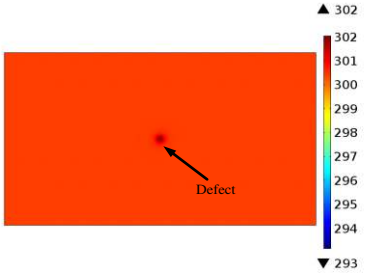


Fig.5 Thermal image in OT

The transient temperature response at a pixel allocated in the defective area is shown in Fig.6.

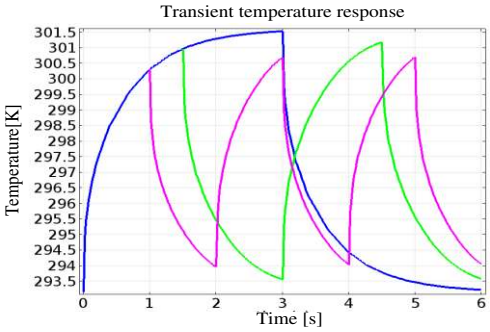


Fig.6 Transient temperature response in OT

In Fig.6, the blue, the green and the pink lines illustrate the transient temperature response of one pulse, two pulses and three pulses, respectively. The maximum temperature rise of two pulses decreases by 6% compared to one pulse, and by 11% in the case of three pulses. Therefore periodic pulsed thermography is capable to decrease temperature rise.

### *C. Data analysis in simulation*

The ECT and OT have the similar transient temperature response and the Fourier Transform is applied to analyze the thermal transient data. As shown in Fig.7, compared to single pulse stimulation, the amplitude and phase spectrum is modulated by periodic pulse. Amplitude and phase spectrum has response on the frequency of $\omega, 3\omega, 5\omega, 7\omega, 9\omega \cdots\cdots$ only, and frequency component 0 is the response of the DC component (constant heat flux). Therefore, the signal resolution is increased. Simultaneously, the resolution can be improved by increasing $\omega$, however, the thermal diffusion length will be decreased according to (5). Therefore, $\omega$ should be chosen to balance defect depth and the resolution.

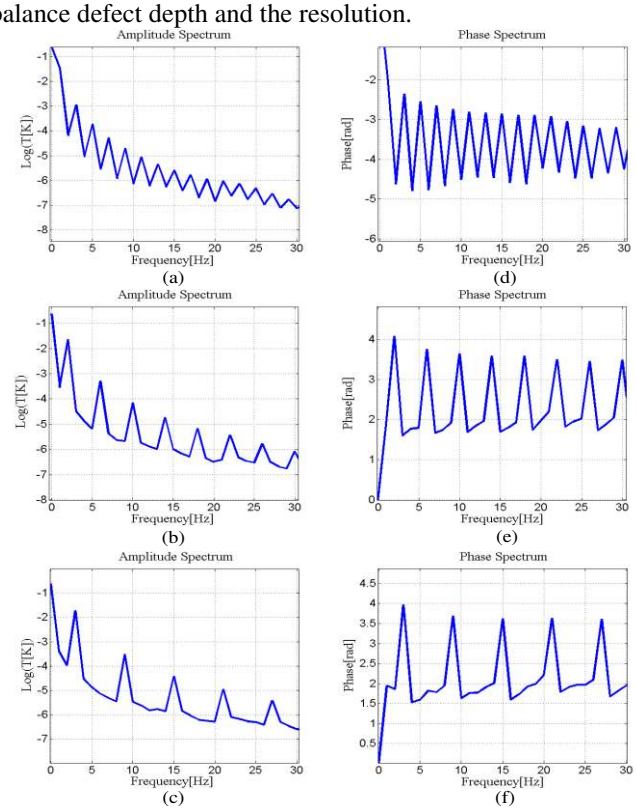


Fig.7 The amplitude spectrum of (a) one pulse; (b) two pulses; (c) three pulses. The phase spectrum of (d) one pulse; (e) two pulses; (f) three pulses.

This article has been accepted for publication in a future issue of this journal, but has not been fully edited. Content may change prior to final publication. Citation information: DOI 10.1109/JSEN.2018.2822290, IEEE Sensors Journal

As discussed in Section III, the simulation result has satisfied the theoretical derivation and verified the feasibility of periodic pulsed thermography. Not withstand above, the simulation result indicated that the periodic pulsed thermography contributes to decrease temperature rise and increase the signal resolution.

## IV. Experiment Set up

### A. Experiment system

The system of eddy current thermography (ECT) and optical thermography (OT) are shown in Fig.8. In ECT, the exciting frequency is 301 kHz. The distance between specimen and coil is 1mm. In OT, the Halogen lamp is selected with the power 1kw. Considering the size of specimen, only one lamp is used. The distance between lamp and specimen is about 0.5m. The IR camera is FLIR A655sc with a high resolution 640× 480 array and a sensitivity of 30$mK$. The sampling frequency is 50Hz.

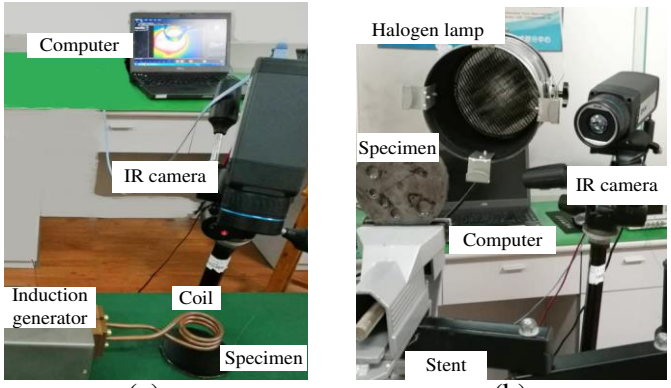


Fig.8 (a) ECT experiment system (b) OT experiment system

### B. Specimen Description

The specimens used in experiment were divided into three groups. Group1 is two layers standard specimen as shown in Fig.9. The depths for 9 defects are constant as 1mm but the size are set as 14,12,10,9,8,7,6,5 and 4 mm, respectively. Nine defects are sequentially numbered as defects 1 to 9 as shown in Table II. The defect is set as through hole which is visualized at the rear side. Emissivity of material has been adjusted by using a classic method of using black paint to make emissivity close to 1.

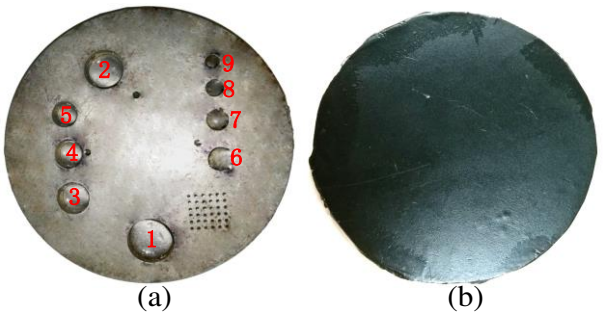


Fig.9 Two layers standard specimen: (a) rear side; (b) front side.

TABLE II:
THE DEFECTS DIMENSIONS AND DEPTHS IN GROUP 1

| Depth | 1mm | | | | | | | | |
|---|---|---|---|---|---|---|---|---|---|
| Number | 1 | 2 | 3 | 4 | 5 | 6 | 7 | 8 | 9 |
| Size[mm] | 14 | 12 | 10 | 9 | 8 | 7 | 6 | 5 | 4 |

Group 2 had two specimens whose defect's size is larger than 10mm. The defect located at the different bonding layer. The defect is set on the adjacent steel layer as shown in Fig.10.The depth of the defects with different layer is about 1mm and 5mm, respectively. Defects are inner defects which is invisible and it located in the center of specimen. The surface was covered with the black paint as well.

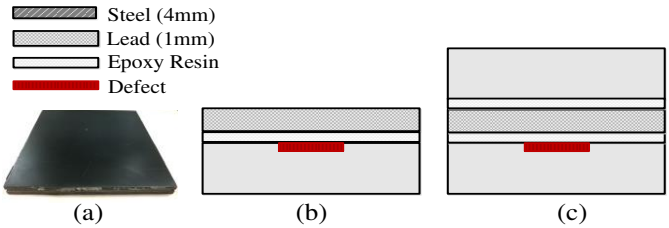


Fig.10 (a) Front view; the sectional view of (b) two layer specimen (c) three layers specimen

Group 3 adopted the specimen of group1 except that the surface was not covered by black paint.

## V. Result and Analysis

### A. Theoretical formula validation

Specimen with a large and shallow defect has chosen for better verification of the theoretical derivation. The experiment adopted the ECT mode and the current was set as 480A. The exciting frequency is 301 kHz, and the sampling frequency is 50Hz. The cycle of pulse is 2s and three pulse have been utilized. The raw data is shown in Fig.11. A pretreatment is applied to the data to subtract the first frame from the temperature sequence.

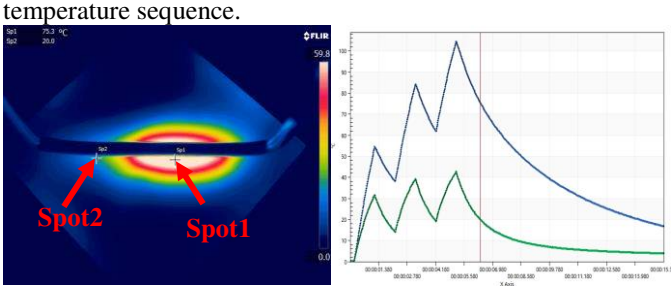


Fig.11 (a) Surface temperature profile; (b) transient response

In Fig.11 (b), the blue line is derived from spot 1 at the defect area, and the green line is from the spot 2 at the non-defect area. The temperature rise in the non-defect region is about 42K which is acceptable in inspection progress of lead-steel bonded structure. The transient response is compared with the curve fitting result as shown in Fig.12. The blue solid line is derived from the experiment data and the red dash line from the curve fitting formula (12).

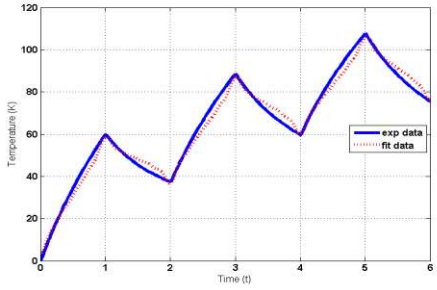


Fig.12 Transient response validation

This article has been accepted for publication in a future issue of this journal, but has not been fully edited. Content may change prior to final publication. Citation information: DOI 10.1109/JSEN.2018.2822290, IEEE Sensors Journal

Both correlation and error analysis have been carried out. It should be noted that all the validation studies have been conducted by Monte Carlo based experiment approach where the process is repeated over 20 realizations. The correlation coefficient is close to 1 and the error is about 0.1.This shows that the proposed theoretical derivation has successfully modelled the periodic pulsed thermography within 10% of error.

Through the Fourier Transform, the frequency spectrum of defect region is shown in Fig.13. This is consistent with the simulation results.

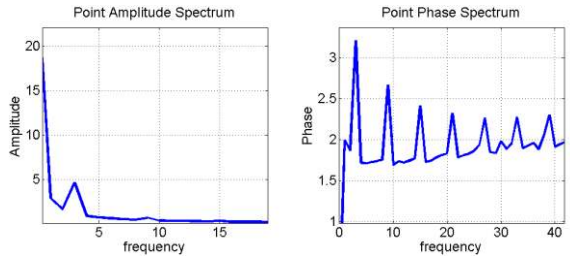


Fig.13 The frequency spectrum of big and shallow defect

The transient response in Fig.11 (b) shows that the temperature rise in defect area is high. A decreased current between 120A and 380A is chosen in subsequent experiment, which is supported by periodic pulsed thermography. A contrast specimen with a small defect has been compared. The raw data is shown in Fig.14.

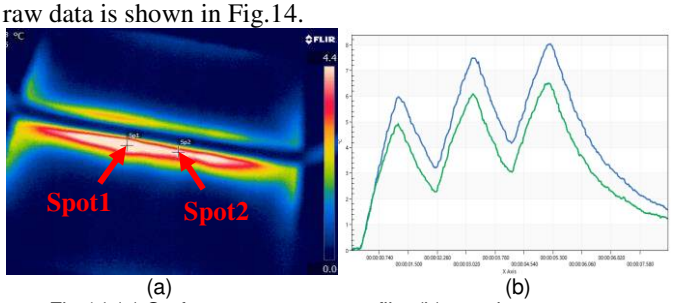


(a) (b)

Fig.14 (a) Surface temperature profile; (b) transient response

The blue line was derived from spot 1 at the defect area, and the green line was from the spot 2 at the non-defect area. The temperature rise is smaller to 10K. Through the Fourier Transform, the frequency spectrum of defect region is shown in Fig.15.

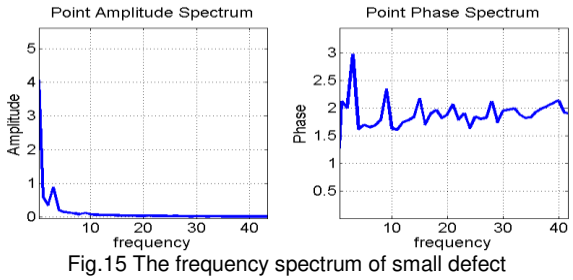


Fig.15 The frequency spectrum of small defect

The result is consistent with the simulation results, except that the sensitivity of phase is decreased.

### *B. Pulsed Thermography versus Periodic Pulsed Thermography*

In order to clearly interpret the detection performance, the results of group 1 was divided into two cases.Case1 contains defects 1 to 7 where periodic time is set as 2s and 6s recordings. In addition, the single pulsed mode is used for comparison where it is set with heating time 3s and the cooling time is 3s. Case 2 includes defects 8 to 9. The periodic time is set as 10s and recording time is 30s in periodic pulsed mode, while the heating time is set as 15 s and cooling time is 15s in single pulse mode.

Case1: single pulsed and periodic-pulsed ECT and optical thermography are compared in the condition of the equal energy. The signal-to-noise ratio (SNR) is calculated for validation. SNR describes the thermal contrast between defective region considered as "signal" and non-defective region defined as "noise" [24]. The calculation of SNR in dB [30] is defined below:

$$SNR = \frac{S}{N} = 20\log_{10}\left(\frac{T_{mD} - T_{mN}}{\sigma(T_{mN})}\right)[dB] \quad (18)$$

where $T_{mD}$ and $T_{mN}$ are average temperature in defective and non-defective regions, respectively. The $\sigma(T_{mN})$ is the temperature standard deviation in the relevant non-defective regions. The results represented in Table III.

TABLE III
RESULT FOR CASE 1 OF GROUP 1

| Group 1 | ECT | OT |
|---|---|---|
| Single pulsed | 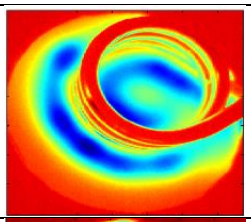 | 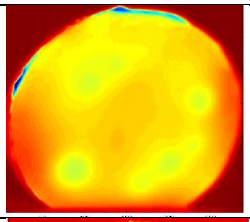 |
| Periodic-pulsed | 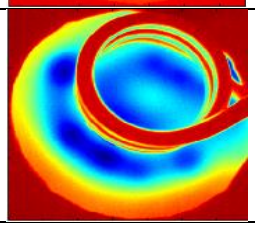 | 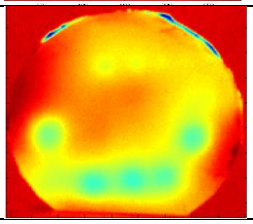 |

Obviously, the SNR is affected by the sound area and uneven heating [25].However, in this work, the SNR is used to compare the single pulse and periodic pulse. In ECT or OT mode, the experiments of single pulse and periodic pulse are implemented at the same condition. This set decreases the effect from location of camera and the observation angle. Therefore, the regions for calculating SNR were basically consistent in the same mode. SNR equal to 0 represents that the defect cannot be detected. The SNR result can be visualized in Table IV and Table V.

TABLE IV
SNR RESULT FOR CASE 1 OF GROUP 1 IN ECT MODE

| SNR | 1 | 2 | 3 | 4 | 5 | 6 | 7 | 8 |
|---|---|---|---|---|---|---|---|---|
| S-pulse | 22.59 | 7.38 | 26.19 | 23.71 | 17.1 | 19.35 | 19.43 | 0 |
| P-pulse | 25.61 | 19.03 | 25.14 | 26.8 | 20.08 | 18.78 | 20.81 | 0 |

TABLE V
SNR RESULT FOR CASE 1 OF GROUP 1 IN OT MODE

| SNR | 1 | 2 | 3 | 4 | 5 | 6 | 7 | 8 |
|---|---|---|---|---|---|---|---|---|
| S-pulse | 32.52 | 28.54 | 25.14 | 26.8 | 25.35 | 21.03 | 15.91 | 0 |
| P-pulse | 27.59 | 25.09 | 21.57 | 22.63 | 18.8 | 17 | 14.99 | 4 |

It indicated that defects from 1 to 7 of case 1 can be detected easily due to the large size. The SNR of defect 8 is 0 except in optical periodic pulsed mode. However, the SNR of defect 8 is lower than 5dB, which is a suspect inspection result. Therefore, 7 defects have been detected in Case 1 with the probability of

This article has been accepted for publication in a future issue of this journal, but has not been fully edited. Content may change prior to final publication. Citation information: DOI 10.1109/JSEN.2018.2822290, IEEE Sensors Journal

detection at 77.8%. Additionally, it demonstrated that the SNR is similar by comparing the single pulse excitation and the proposed periodic pulse excitation except defect 2 in ECT mode. The SNR of defect 2 in single pulse is 12*dB* which is less than that of the periodic pulse. It shows that periodic pulsed thermography is less sensitivity to local uneven heating.

Furthermore, through the comparison of ECT and OT, the SNR is similar and relevant to the defect size. However, defect 2 had a large fluctuation in ECT. The reason is that the defect locates away from the valid detection range which is constrained by the shape of the coil. Simultaneously, the ECT had coil masking problem as shown in Table III. Therefore, the OT is adopted.

Case2：According to the empirical value, the defect can be detected when size-to-depth ratio larger than 2:1 [26-27]. Therefore the defects 8 to 9 for case 2 can be detected theoretically. Previous studies have indicated that increase the injected energy can increase the detectability [28]. Therefore, in order to detect defect 8 to 9, more energy was injected to specimen in case2. Unfortunately, single pulsed mode destroyed the specimen or led to disbond due to large energy as shown in Fig.16.

Fig.16 the destroyed specimen

Therefore, only periodic-pulsed mode can be applied for Case 2. All the defects in Case2 were successfully detected as shown in Fig.17. The SNR values have been represented in Table.VI. It noted that the SNR for defects 6 to 9 is close to 15*dB*. Therefore, in combination this to Case1, all the defects in group 1 can be detected with periodic pulsed thermography mode with probability of detection equals to 100%.

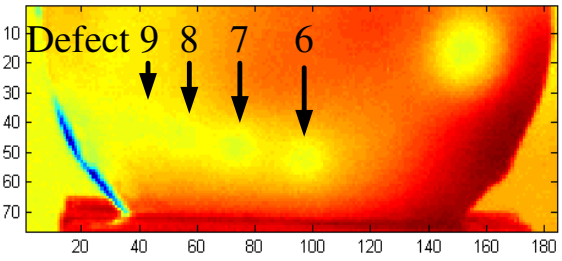


Fig.17 Result of case 2;

TABLE VI

SNR RESULT FOR CASE 2 OF GROUP 1 IN OT MODE

| SNR | 6 | 7 | 8 | 9 |
|---|---|---|---|---|
| p-pulse | 16.12 | 18.39 | 15.61 | 15.51 |

### C. Feasibility study of deep defect detection

The results of group 2 were shown in Table VII and the defect can be detected. All defect of group2 was visualized and the sensitivity of optical thermography is higher than ECT method. It indicates that the periodic pulsed thermography is suitable for detection of the deeper defects in multilayer specimen.

TABLE VII

EXPERIMENT RESULT OF GROUP 2

| Group 2 | ECT | OT |
|---|---|---|
| wo layers | 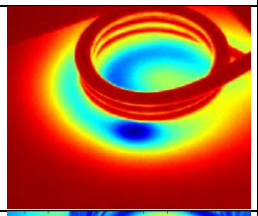 | 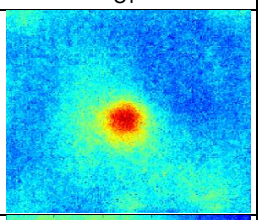 |
| hree layers | 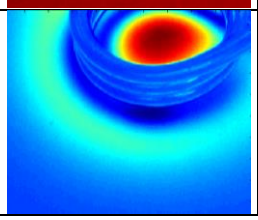 | 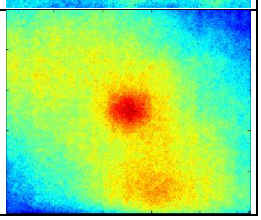 |

### D. The influence of emissivity

In application, the surface of the sample may not be allowed to cover the black paint. Therefore, the influence of surface emissivity should be considered. Fig.18 represented the result of group 3 which the sample is under testing without painting. The optical thermography cannot detect defects due to the strong influence from the emissivity and the reflection while ECT shows the potential ability to detect defects due to the local volume induction heat that penetrate inner depth on the lead layer. Thus, the ECT will result inner heating by ways of eddy current penetration. Therefore the defect can be detected despite the emissivity variation.

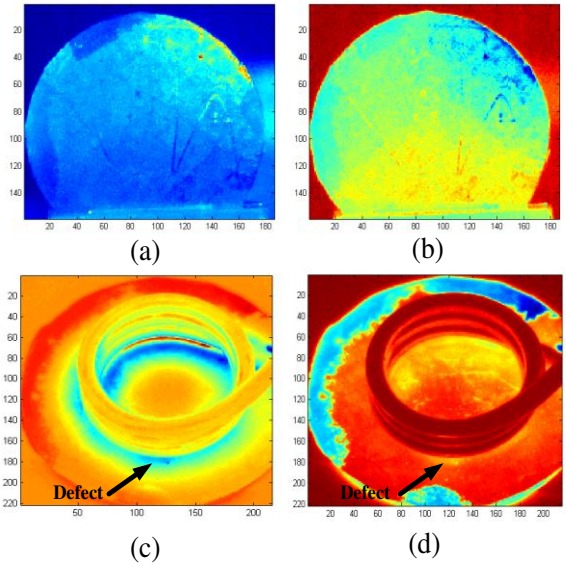


Fig.18 The amplitude and phase spectrum of optical thermography (a), (b) and ECT(c), (d)

In summary, for detection of multilayer lead-steel bonded structure, periodic pulsed thermography can detect smaller defect than single pulsed thermography and it has the potential to detect deep flaws of multi-layer while preventing specimen from destruction. At the same time, periodic pulsed thermography has the advantages of high signal-to-noise resolution and less sensitivity to local uneven heating. OT has the advantages of larger detection region and no masking compared to ECT. However, OT cannot inject enough energy to specimen without black paint. Thus, the performance of OT is highly influenced by surface's uneven emissivity.

This article has been accepted for publication in a future issue of this journal, but has not been fully edited. Content may change prior to final publication. Citation information: DOI 10.1109/JSEN.2018.2822290, IEEE Sensors Journal

### *E. The quantitative analysis*

The region growing method is utilized to segment and extract defects. Region growing is a region-based image segmentation method. The progress examines the neighboring pixels of initial seed points and determines whether the pixel neighbors should be added to the region [29]. Size expansion rate (SER) is defined to evaluate the accuracy of detection. The size expansion rate is closer to 1, indicating that the detected defect shape is closer to the actual defect shape.

$$SER = S_d / S_a \tag{19}$$

where the $S_d$ and $S_a$ is the detection area and the actual area, respectively.

The region growing method is utilized to segment the result of the OT mode, due to the ECT mode has the coil masking problem. The segmentation process of group1 included two parts. The Fig.19 (a) is the segmentation of the defects 1 to 5, the raw data is from OT result of the table III. The Fig.19 (b) is the segmentation of the defects 6 to 9, the raw data is from Fig.18. The SER of group 1 is represented in Table VIII.

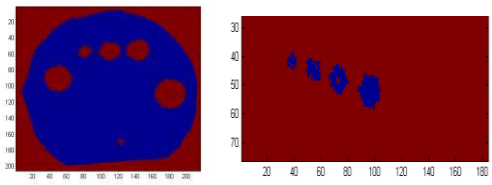

(a) (b)

Fig.19 The segmentation results of (a) defects 1-5; (b) defects 6-9

TABLE VIII:

SER RESULT FOR GROUP 1 IN OT MODE

| Num | 1 | 2 | 3 | 4 | 5 | 6 | 7 | 8 | 9 |
|---|---|---|---|---|---|---|---|---|---|
| SER | 1.15 | 1.36 | 1.21 | 1.23 | 0.56 | 1.14 | 1.05 | 0.96 | 1.2 |

The segmentation results of group 2 is shown in Fig.20. The SER of group 2 is represented in Table IX. The raw data is from OT results of the table VII.

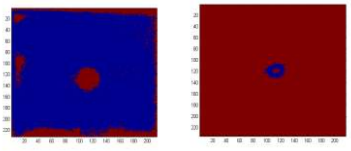

(a) (b)

Fig.20 The segmentation result of defect (a) at the first bonding layer; (b) at the second bonding layer

TABLE IX:

SER RESULT FOR GROUP 2 IN OT MODE

| Depth | 1mm | 5mm |
|---|---|---|
| SER | 2.5069 | 1.14 |

## VI. CONCLUSION

In this paper, a novel approach of periodic pulsed thermography was proposed for detection of the lead-steel bonded structure. The theory derivation and the simulation indicated the detection feasibility and verified that periodic pulsed thermography have the advantages of decreasing instantaneous temperature rise and increasing signal to noise resolution. Experiment studies verified that the periodic pulsed thermography is effective to small defect detection. In addition, the validation and comparison on both eddy current and optical excitation mode have been conducted.

The OT has advantages of large detection region without any cover compared to ECT. However, the emissivity problem exists since the OT cannot heat the specimen due to the high reflection without painting. ECT can inject heat to inner specimen and shows potential in solving the problem of uneven emissivity. The investigation of eddy current and optical excitation modes for complex geometry samples will be conducted in future work.

## ACKNOWLEDGMENT

The work was supported by NSAF (Grant No. U1430115).

## REFERENCES

[1] R. D. Adams and B. W. Drinkwater, "Nondestructive testing of adhesively-bonded joints," *International Journal of Materials & Product Technology,* vol. 30, pp. 385-398, 1997.

[2] N. Montinaro, D. Cerniglia, G. Pitarresi, "Detection and characterisation of disbonds on Fibre Metal Laminate hybrid composites by flying laser spot thermography," Compos. Part B Eng, vol. 108 pp. 164–173, 2017

[3] Cerniglia D, Pantano A, Montinaro N, " 3D simulations and experiments of guided wave propagation in adhesively bonded multi-layered structures," NDT&E International, vol. 43, pp. 527-535, 2010.

[4] Tighe R C, Dulieu-Barton J M, Quinn S, "Infrared Techniques for Practical Defect Identification in Bonded Joints in Liquefied Natural Gas Carriers," Experimental Techniques, vol. 4, 2017.

[5] C. C. H. Guyott, P. Cawley, R. D. Adams, "The Non-destructive Testing of Adhesively Bonded Structure: A Review," Journal of Adhesion, vol. 20(2), pp. 129-159, 1986.

[6] King W. G, "A practical introduction to magnetic particle testing : Basic rules for satisfactory detection," Non-Destructive Testing, vol. 1(2), pp. 84-90, 1967.C. J. Brotherhood, B. W. Drinkwater, and S. Dixon, "The detectability of kissing bonds in adhesive joints using ultrasonic techniques," Ultrasonics, vol. 41, pp. 521-529, 2003.

[7] D. Yan, B. W. Drinkwater, and S. A. Neild, "Measurement of the ultrasonic nonlinearity of kissing bonds in adhesive joints," Ndt & E International, vol. 42, pp. 459-466, 2009.

[8] S. Dixon, C. Edwards, and S. B. Palmer, "The Analysis of Adhesive Bonds Using Electromagnetic Acoustic Transducers," Ultrasonics, vol. 32, pp. 425-430, 1995.

[9] I. Amenabar, A. Mendikute, A. López-Arraiza, M. Lizaranzu, and J. Aurrekoetxea, "Comparison and analysis of non-destructive testing techniques suitable for delamination inspection in wind turbine blades," Composites Part B, vol. 42, pp. 1298-1305, 2011.

[10] L. Balaji, K. Balasubramaniam, and C. V. Krishnamurthy, "Induction thermography for non-destructive evaluation of adhesive bonds," vol. 1511, pp. 579-586, 2013.

[11] R. C. Waugh, J. M. Dulieubarton, and S. Quinn, "Pulse Phase Thermography and its Application to Kissing Defects in Adhesively Bonded Joints," Applied Mechanics & Materials, vol. 70, pp. 369-374, 2011.

[12] Tighe R C, Dulieu-Barton J M, Quinn S, "Identification of kissing defects in adhesive bonds using infrared thermography," 《International Journal of Adhesion & Adhesives》 vol. 64, 2016.

[13] J. M. Roche, "Common tools for quantitative time-resolved pulse and step-heating thermography – part I: theoretical basis," Quantitative Infrared Thermography Journal, vol. 11, pp. 43-56, 2014.

[14] X. Maldague, "Introduction to NDT by active infrared thermography," Materials Evaluation, vol. 60, pp. 1060-1073, 2002.

[15] C. Ibarra-Castanedo and X. P. V. Maldague, Infrared Thermography: Springer Berlin Heidelberg, 2013.

[16] Y. He, M. Pan, D. Chen, G. Tian, and H. Zhang, "Eddy current step heating thermography for quantitatively evaluation," Applied Physics Letters, vol. 103, pp. 023112-2698, 2013.

[17] D. Wu and G. Busse, "Lock-in thermography for nondestructive evaluation of materials," Revue Générale De Thermique, vol. 37, pp. 693-703, 1998.

[18] Y. He, G. Y. Tian, M. Pan, and D. Chen, "Eddy current pulsed phase thermography and feature extraction," Applied Physics Letters, vol. 103, pp. 084104-084104-4, 2013.

[19] Y. He, M. Pan, G. Tian, D. Chen, Y. Tang, and H. Zhang, "Eddy current pulsed phase thermography for subsurface defect quantitatively evaluation," Applied Physics Letters, vol. 103, pp. 054103-2120, 2013.

[20] R. Mulaveesala and S. Tuli, "Theory of frequency modulated thermal wave imaging for nondestructive subsurface defect detection," Applied Physics Letters, vol. 89, p. 492, 2006.
[21] C. Ibarracastanedo, M. Klein, S. Vallerand, and X. P. Maldague, "Thermographic nondestructive evaluation: overview of recent progress," Proceedings of SPIE - The International Society for Optical Engineering, vol. 5073, pp. 450-459, 2003.
[22] X. Maldague, A. Ziadi, and M. Klein, "Double pulse infrared thermography," Ndt & E International, vol. 37, pp. 559-564, 2004.
[23] J. Liu, W. Yang, and J. Dai, "Research on thermal wave processing of lock-in thermography based on analyzing image sequences for NDT," Infrared Physics & Technology, vol. 53, pp. 348-357, 2010.
[24] Y. T. Gui, Y. Gao, K. Li, Y. Wang, B. Gao, and Y. He, "Eddy Current Pulsed Thermography with Different Excitation Configurations for Metallic Material and Defect Characterization," Sensors, vol. 16, p. 843, 2016.
[25] J. F. Florez-Ospina and H. D. Benitez, "From local to global analysis of defect detectability in infrared non-destructive testing," Infrared Physics & Technology, vol. 63, pp. 211-221, 2014.
[26] Maldague X P V., "Theory and Practice of Infrared Technology for Nondestructive Testing," Chapter, vol. 4(3), p. 307, 2001.
[27] F. D. C. Badghaish A A, "Non-destructive Inspection of Composites Using Step Heating Thermography," Journal of Composite Materials, vol. 42(13), pp. 1337-1357, 2008.
[28] Xiaoxi Li, Bin Gao, Guangping Tang, "Feasibility study of debonding NDT for multi-layer metal-metal bonding structure by using eddy current pulsed thermography," Technology & Application Forum 2017.
[29] B. L. Adams R, "Seeded Region Growing," IEEE Transactions on Pattern Analysis & Machine Intelligence, vol. 16(6), pp. 641-647, 2002.
[30] H. Zhang, S. Sfarra, F. Sarasini, C. Castanedo, S. Perilli, H. Fernandes, Y. Duan, J. Peeters, N. P. Avdelidis, X. Maldague 'Optical and Mechanical Excitation Thermography for Impact Response in Basalt-Carbon Hybrid Fiber-Reinforced Composite Laminates', IEEE Transactions on Industrial Informatics (2018) 14(2): 514-522.

**Xiaoxi Li** (M' 12-SM' 14) received his B.Sc. degree from the School of Nanchang University (2011-2015), Nanchang, China. He is currently pursuing the M.Sc. degree in Research Center of Non-destructive Evaluation and Structural Health Monitoring at the University of Electronic Science and Technology of China, Chengdu, China. His research interests nondestructive testing and evaluation

**Bin Gao** (M' 12-SM' 14) received his B.Sc. degree in communications and signal processing from Southwest Jiao Tong University (2001-2005), China, MSc degree in communications and signal processing with Distinction and PhD degree from Newcastle University, UK (2006-2011). He worked as a Research Associate (2011-2013) with the same university on wearable acoustic sensor technology. Currently, he is a Professor with the School of Automation Engineering, University of Electronic Science and Technology of China (UESTC), Chengdu, China. His research interests include sensor signal processing, machine learning, social signal processing, nondestructive testing and evaluation where he actively publishes in these areas. He is also a very active reviewer for many international journals and long standing conferences. He has coordinated several research projects from National Natural Science Foundation of China

**Yuyu Zhu** received his B.S. degree in automation from University of Science and Technology (1998-2002), China, MSc degree in control theory and control engineering (2006-2009) with the same university. He works as a Associate Professor in this school on monitoring and control technology and power electronics technology. Currently, he is a PhD student in University of Electronic Science and Technology of China (UESTC). His research interests include nondestructive testing and evaluation, power electronics technology.

**Wai Lok Woo** was born in Malaysia. He received the BEng degree (1st Class Hons.) in Electrical and Electronics Engineering and the PhD degree from the Newcastle University, UK. He was awarded the IEE Prize and the British Scholarship to continue his research work. He is currently a Senior Lecturer and Director of Operations with the Sc hool of Electrical and Electronic Engineering. His major research is in the mathematical theory and algorithms for nonlinear signal and image processing. This includes areas of machine learning for signal processing, blind source separation, multidimensional signal processing, signal/image deconvolution and restoration. He has an extensive portfolio of relevant research supported by a variety of funding agencies. He has published over 250 papers on these topics on various journals and international conference proceedings. Currently, he is Associate Editor of several international journals and has served as lead-editor of journals' special issues.

**Gui Yun Tian** (M'01-SM'03) received the B.Sc. degree in metrology and instrumentation and M.Sc. degree in precision engineering from the University of Sichuan, Chengdu, China, in 1985 and 1988, respectively, and the Ph.D. degree from the University of Derby, Derby, U.K., in 1998. From 2000 to 2006, he was a Lecturer, Senior Lecturer, Reader, Professor, and Head of the group of Systems Engineering, respectively, with the University of Huddersfield, U.K. Since 2007, he has been based at Newcastle University, Newcastle upon Tyne, U.K., where he has been Chair Professor in Sensor Technologies. Currently, He is also an adjunct professor with School of Automation Engineering, University of Electronic Science and Tech nology of China. He has coordinated several research projects from the Engineering and Physical Sciences Research Council (EPSRC), Royal Academy of Engineering and FP7, on top of this he also has good collaboration with leading industrial companies such as Airbus, Rolls Royce, BP, nPower, Networkrail and TWI among others.

**Jianwen Li** received the M.Sc. degree from the School of Materials science professionals, Sichuan University, China, in 2001. Currently, he is a senior engineer with Institute of Machinery Manufacturing Technology, China Academy of Engineering Physics (CAEP), Mianyang, China. His research interests include nondestructive testing technologies of matel materials.

**Guangping Tang** received his B.Sc. degree in material science and engineer from Zhejiang University (1987-1991), Hangzhou, China, and M.Sc degree in mechanical engineer Sichuan University (2000-2003), Chengdu, China. Since 1991, he has been working as a researcher in China Academy of Engineer Physics, Mianyang, Sichuan Province. His research interests include engineer materials, functional materials, surface modification with laser

.**Chaoming Sun** received the M.Sc. degree from the School of Mechatronic Engineering and Automation, Shanghai University, China, in 2002.Currently, he is a senior engineer with Institute of Machinery Manufacturing Technology, China Academy of Engineering Physics (CAEP), Mianyang, China.